J Bio Tribo Corros (2016) 2:1
DOI 10.1007/s40735-015-0031-y

ORIGINAL PAPER

# Investigation of Thermodynamic Parameters for Steel Corrosion in Acidic Solution in the Presence of *N*,*N*′-Bis(phloroacetophenone)-1,2 propanediamine

**Farhad Mohsenifar[1] · Hojat Jafari[2] · Koray Sayin[3]**

Received: 28 September 2015 / Revised: 19 November 2015 / Accepted: 2 December 2015 / Published online: 8 January 2016


**Abstract** *N*,*N*′-Bis(phloroacetophenone)-1,2-propanediamine as corrosion inhibitor for steel in hydrochloric acid has been studied using electrochemical techniques and surface techniques. Results showed that the inhibition occurs through adsorption of the inhibitor molecules on the metal surface. The inhibition efficiency was found to increase with increasing inhibitor concentration and decreased with increasing temperature. Thermodynamic parameters for adsorption and activation processes were determined. Polarization data indicated that this compound acts as the mixed-type inhibitor and the adsorption basically obeys the Langmuir adsorption isotherm. The quantum chemical calculations were performed at the density functional theory level using B3LYP functional with the 6-31G (d,p).

**Keywords** Metals · Thermodynamic properties · Adsorption · Corrosion · Electrochemical techniques · Computational techniques

✉ Hojat Jafari
hojatjafari80@yahoo.com

[1] Department of Mechanical Engineering, Higher Education Complex of Bam, Bam, Kerman, Iran

[2] Abadan Faculty of Petroleum Engineering, Petroleum University of Technology, Abadan, Iran

[3] Department of Chemistry, Institute of Science, Cumhuriyet University, 58140 Sivas, Turkey

## 1 Introduction

Corrosion is worth investigating in oilfield applications, because corrosion problems represent a large portion of the total costs for oil and gas producing companies every year worldwide [1]. Even with advanced corrosion-resistant materials available, carbon steel has been widely employed as the construction material for pipe works in the oil and gas production such as downhole tubular flow lines and transmission pipelines. Steel pipelines play an important role in transporting gases and liquids throughout the world [2]. Moreover, appropriate corrosion control can help avoid many potential disasters that can cause serious issues including loss of life, negative social impacts, and water resource and environmental pollution [3, 4].

Among the corrosion control techniques, the development of new corrosion inhibitors have substantially increased in the recent years because it is believed to be one of the most effective and economic methods to protect metal corrosion in acidic media [5, 6]. Most of the well-known acid inhibitors are organic compounds containing N, O, P, S, and aromatic ring or triple bonds. It was reported before that the inhibition efficiency decreases in the order: O < N < S < P [6]. In general, organic compounds are effective inhibitors of aqueous corrosion of many metals and alloys. The use of chemical inhibitors to decrease the rate of corrosion processes of carbon steels is quite varied [5–9]. A variety of organic compounds containing heteroatoms such as O, N, S, and multiple bonds in their molecule are of particular interest as they give better inhibition efficiency than those containing N or S alone [10]. Sulfur- and/or nitrogen-containing heterocyclic compounds with various substituents are considered to be effective corrosion inhibitors.

The presence of –C=N– group in Schiff base molecules enhances their adsorption ability and corrosion inhibition efficiency [2, 7]. Adsorption of inhibitors on the metal surface involves the formation of two types of interaction (physical adsorption and chemical adsorption). Physical adsorption requires the presence of both electrically charged surfaces of the metal and charged species in the bulk solution. The chemisorption process involves charge sharing or charge transfer from the inhibitor molecules to the metal surface to form a coordinate-type bond and takes place in the presence of heteroatoms (P, N, S, O, etc.) with lone pairs of electrons and/or aromatic ring in the molecular structure [2, 7].

Density functional theory (DFT) has grown to be a useful theoretical method to interpret experimental results, enabling one to obtain structural parameters for even huge complex molecules, and it can explain the hard and soft acid–base (HSAB) behavior of organic molecules, i.e., DFT connects some traditional empirical concepts with quantum mechanical interpretations [9, 10]. Therefore, DFT is a very powerful technique to probe the inhibitor/surface interaction and to analyze experimental data. These are the reasons why we selected both electrochemical and DFT methods to evaluate the efficiency of *N*,*N*′-bis(phloroacetophenone)-1,2-propanediamine (PPPD).

Thus, the present work deals with the corrosion inhibition analysis of PPPD in the corrosive medium (HCl). In addition to spectroscopic and electrochemical techniques like SEM, AFM, polarization curve, and electrochemical impedance, Quantum chemical calculations have been performed using DFT, and several quantum chemical indices are calculated and correlated with the inhibitive effect of (PPPD).

## 2 Experimental

### 2.1 Materials

The material tested was a carbon steel sample, which was cut from the parent pipe with chemical composition reported as C: 0.2, Si: 0.032, P: 0.21, Mn: 0.35 % w, Fe: Rest. The specimens of dimension 1 cm × 1 cm (exposed) × 4.3 mm (isolated with polyester resin) were used for polarization and electrochemical impedance methods. The exposed areas of the electrodes were mechanically abraded with 220, 600, 1000, and 2000 grades of emery paper, degreased with acetone and rinsed with distilled water before each electrochemical experiment.

The aggressive solution of 1 M HCl was prepared by dilution of Merck Product HCl. The concentration range of inhibitors employed varied from $1 \times 10^{-4}$ to $5 \times 10^{-3}$ M. All chemicals used in the present work were reagent-grade Merck products and used as received without further purification. The PPPD Schiff base (Fig. 1) was prepared in moderate yield (92 %) by the condensation of 2,4,6-trihydroxyacetophenone monohydrate (2 mmol) with propylenediamine (1 mmol) in a stirred ethanolic solution and heated to reflux for 2 h according to the described procedure [11].

### 2.2 Methods

The apparatus for electrochemical investigations consists of computer-controlled Auto Lab potentiostat/galvanostat (PGSTAT302N) corrosion measurement system at a scan rate of 1 $mVS^{-1}$. The electrochemical experiments were carried out using a conventional three-electrode cell assembly at 25 °C. A rectangular platinum foil was used as counter electrode and saturated calomel electrode as the reference electrode. The EIS experiments were conducted in the frequency range of 100 kHz–0.01 Hz at open circuit potential. The AC potential amplitude was 10 mV. Time interval of 25–30 min was given for steady-state attainment of open circuit potential.

The Steel specimens of size 1 cm × 1 cm × 0.43 cm were abraded with emery paper (up to 2000) to give a homogeneous surface, and then washed with distilled water and acetone. The specimens were immersed in 1 M HCl prepared with and without addition of $2 \times 10^{-3}$ M at 25 °C for 6 h, cleaned with distilled water. The surface morphology of the electrode surface was evaluated by scanning electron microscopy (VEGA) and atomic force microscopy (AFM) Nanosurf Easyscan 2.

Numerical calculations were done by using Gaussian package program [12, 13] and representation of figures which are related with computational chemistry was prepared by using ChemBioDraw Ultra Version (13.0.0.3015) [14]. M06-2X method was selected as method with 6-31G basis set for calculations. All calculations were done in vacuum and the vibration frequency analyses were indicated that optimized structures of investigated inhibitors are at stationary points corresponding to local minima without imaginary frequencies. Mentioned quantum chemical descriptors were calculated by using Eqs. (1)–(17) [15–21].

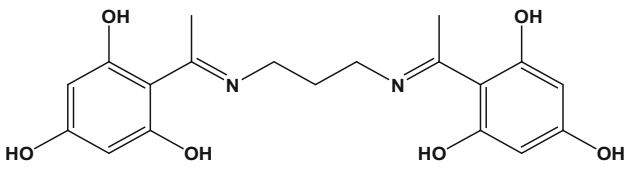


**Fig. 1** Chemical structure of PPPD

$$E_{GAP} = E_{LUMO} - E_{HOMO}, \quad (1)$$

$$I = -E_{HOMO}, \quad (2)$$

$$A = -E_{LUMO}, \quad (3)$$

$$\eta = \frac{I - A}{2}, \quad (4)$$

$$\sigma = \frac{1}{\eta}, \quad (5)$$

$$\chi = \frac{|E_{HOMO} + E_{LUMO}|}{2}, \quad (6)$$

$$\mu = -\chi, \quad (7)$$

$$\omega = \frac{\mu^2}{2\eta}, \quad (8)$$

$$N = \frac{1}{\omega}, \quad (9)$$

$$f_k^+ = P_k(N+1) - P_k(N), \quad (10)$$

$$f_k^- = P_k(N) - P_k(N-1), \quad (11)$$

$$f_k^0 = \frac{P_k(N+1) - P_k(N-1)}{2}, \quad (12)$$

$$\sigma^+ = \sigma x f_k^+, \quad (13)$$

$$\sigma^0 = \sigma x f_k^0, \quad (14)$$

$$\sigma^- = \sigma x f_k^-, \quad (15)$$

$$E_{H^+} = E_{H_3O^+} - E_{H_2O}, \quad (16)$$

$$PA = E_{pro.inh.} - (E_{non-pro.inh.} + E_{H^+}), \quad (17)$$

where $E_{H^+}$, $E_{H_3O^+}$, $E_{H_2O}$, $E_{pro.\ inh.}$, $E_{non\text{-}pro.\ inh.}$, and PA are total energy of proton, total energy of hydronium, total energy of water, total energy of protonated inhibitor, total energy of non-protonated inhibitor, and proton affinity, respectively.

## 3 Results and Discussion

### 3.1 Electrochemical Results

Polarization curves were obtained for carbon steel in 1 M HCl solution with and without inhibitors. The polarization exhibits Tafel behavior. Tafel lines obtained at various concentrations of PPPD in 1 M HCl solutions are shown in Fig. 2, at 25 °C, respectively. The corresponding electrochemical parameters, i.e., corrosion potential ($E_{corr}$ vs. SCE), corrosion current density ($I_{corr}$), cathodic and anodic Tafel slopes ($\beta_a$, $\beta_c$), and the degree of surface coverage ($\theta$) values were calculated from these curves and are given in Table 1. The degree of surface coverage for different

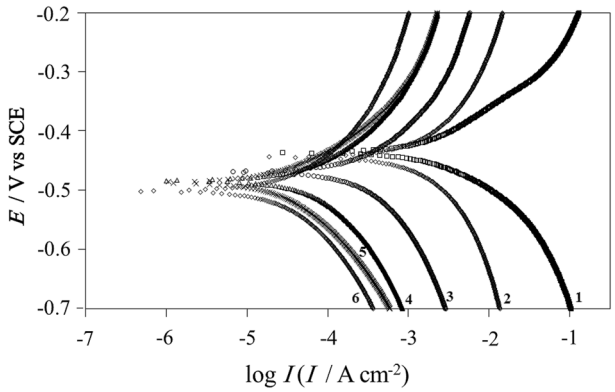


**Fig. 2** Anodic and cathodic polarization curves for carbon steel in 1 M HCl without and with various concentration of PPPD at 25 °C: (*1*) 0 M, (*2*) $1 \times 10^{-4}$ M, (*3*) $3 \times 10^{-4}$ M, (*4*) $5 \times 10^{-4}$ M, (*5*) $1 \times 10^{-3}$ M, (*6*) $2 \times 10^{-3}$ M

concentrations of inhibitor is calculated using the following equations [22, 23]:

$$\theta = \frac{I - \dot{I}}{I}, \quad (18)$$

where $I$ and $\dot{I}$ are the corrosion current densities without and with corrosion inhibitor, respectively, determined by the intersection of the extrapolated Tafel lines at the corrosion potential for carbon steel in uninhibited and inhibited acid solution. The presence of PPPD shifts both anodic and cathodic branches to the lower values of current densities and thus causes a remarkable decrease in the corrosion rate. It can be clearly seen from Fig. 2 that both anodic metal dissolution of iron and cathodic hydrogen and oxygen evolution reactions were inhibited after the addition of Schiff base to the aggressive solution. This result is indicative of the adsorption of inhibitor molecules on the active sites of carbon steel surface [24]. The inhibition of both anodic and cathodic reactions is more pronounced with the increasing inhibitor concentration. However, the influence is more pronounced in the cathodic polarization plots compared to that of the anodic polarization plots. The cathodic current–potential curves (Fig. 2) giving rise to parallel lines indicate that the addition of PPPD to the 1 M HCl solution does not modify the reduction mechanism and the reduction at carbon steel surface takes place mainly through a charge transfer mechanism [25–27]. The slopes do not display an order with the inhibitor concentration; this feature indicates that inhibition occurred by a blocking mechanism on the available metal spaces [28–31]. The corrosion potential displayed a small change in the range of −451 to −513 mV versus SCE and curves changed slightly toward the negative direction (Fig. 2). These results indicated that the presence of PPPD compounds inhibited iron oxidation and to a lower extent hydrogen evolution;

**Table 1** Potentiodynamic polarization parameters for the corrosion of Steel in 1 M HCl solution in the absence and in the presence of different concentrations of PPPD at 25 °C

| Concentration, M | $E_{corr}$ (±1), mV | $I_{corr}$ (±5), μA cm$^{-2}$ | $\beta a$ (±1), mV dec$^{-1}$ | $-\beta c$ (±1), mV dec$^{-1}$ | $R_p$ (±1), Ω cm$^2$ | $\theta$ (±10$^{-2}$) |
|---|---|---|---|---|---|---|
| Blank | 451 | 316 | 80 | 111 | 396 | – |
| $1 \times 10^{-4}$ | 463 | 158 | 82 | 113 | 816 | 0.49 |
| $3 \times 10^{-4}$ | 479 | 100 | 83 | 117 | 1240 | 0.68 |
| $5 \times 10^{-4}$ | 493 | 79 | 86 | 118 | 1724 | 0.74 |
| $1 \times 10^{-3}$ | 502 | 63 | 83 | 121 | 1859 | 0.80 |
| $2 \times 10^{-3}$ | 513 | 20 | 81 | 122 | 5473 | 0.93 |

consequently, these compounds can be classified as mixed corrosion inhibitors, as electrode potential displacement is lower than 85 mV in any direction [32]. The polarization resistance ($R_p$) from Tafel extrapolation method was calculated using the Stern–Geary Equation (Eq. 19) [33].

$$R_p = \frac{\beta a \cdot \beta c}{2.303\ (\beta a + \beta c)} \times \frac{1}{I_{corr}} \tag{19}$$

By increasing the inhibitor concentration, the polarization resistance increases in the presence of compound, indicating adsorption of the inhibitor on the metal surface to block the active sites efficiently and inhibit corrosion [34].

Figure 3 shows the Nyquist diagrams of carbon steel in 1 M HCl solutions containing different concentrations of PPPD at 25 °C, respectively. All the impedance spectra exhibit single depressed semicircle. The diameter of semicircle increases with the increase of PPPD concentration. The semicircular appearance shows that the corrosion of carbon steel is controlled by the charge transfer and the presence of PPPD does not change the mechanism of carbon steel dissolution [35, 36]. In addition, these Nyquist diagrams are not perfect semicircles. The deviation of semicircles from perfect circular shape is often referred to the frequency dispersion of interfacial impedance [37–40]. This behavior is usually attributed to the inhomogeneity of the metal surface arising from surface roughness or interfacial phenomena, which is typical for solid metal electrodes [41]. The equivalent circuit compatible with the Nyquist diagram recorded in the presence of inhibitor is depicted in Fig. 4. The simplest approach requires the theoretical transfer function $Z(\omega)$ to be represented by a parallel combination of a resistance $R_{ct}$ and a capacitance $C$, both in series with another resistance $R_s$ [42].

$$Z(\omega) = Rs + \frac{1}{\frac{1}{R_{ct}} + i\omega C}, \tag{20}$$

where $\omega$ is the frequency in rad/s, $\omega = 2\pi f$, and $f$ is the frequency in Hz. To obtain a satisfactory impedance simulation of steel, it is necessary to replace the capacitor ($C$) with a constant phase element (CPE) $Q$ in the equivalent circuit. The most widely accepted explanation for the presence of CPE behavior and depressed semicircles on solid electrodes is microscopic roughness, causing an inhomogeneous distribution in the solution resistance as well as in the double-layer capacitance [43]. CPE $Q_{dl}$, $R_s$, and $R_{ct}$ can be corresponded to double-layer capacitance, $Q_{dl} = R^{n-1}C_{dl}^{n}$ solution resistance, and charge transfer resistance, respectively. To corroborate the equivalent circuit, the experimental data are fitted to equivalent circuit and the circuit elements are obtained. Table 2 illustrates the equivalent circuit parameters for the impedance spectra of corrosion of steel in 1 M HCl Solution. The data indicate that increasing charge transfer resistance is associated with a decrease in the double-layer capacitance. It has been

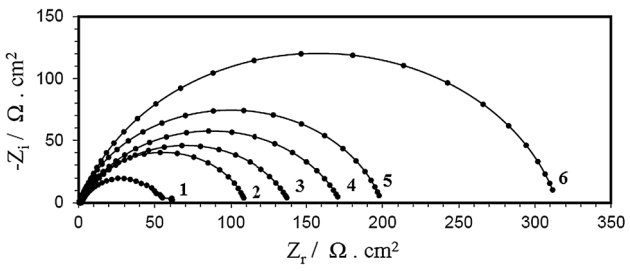


**Fig. 3** Nyquist plots for carbon steel in 1 M HCl without and with various concentration of PPPD at 25 °C: (*1*) 0 M, (*2*) $1 \times 10^{-4}$ M, (*3*) $3 \times 10^{-4}$ M, (*4*) $5 \times 10^{-4}$ M, (*5*) $1 \times 10^{-3}$ M, (*6*) $2 \times 10^{-3}$ M

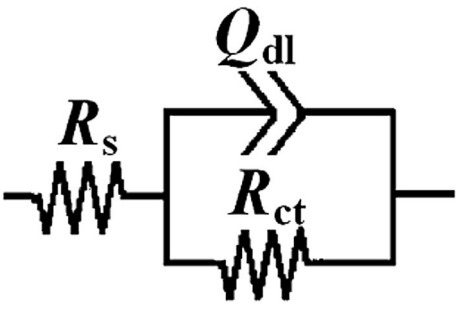


**Fig. 4** Equivalent circuits compatible with the experimental impedance data in Fig. 3 for corrosion of steel electrode at different inhibitor concentrations

**Table 2** Impedance data for steel in 1 M HCl solution without and with different concentrations of PPPD at 25 °C

| Concentration, M | $R_s$ ($\pm10^{-1}$), Ω cm$^2$ | $R_{ct}$ ($\pm1$), Ω cm$^2$ | $Q_{dl}$ ($\pm10^{-3}$), F cm$^2$ | $C_{dl}$ ($\pm10^{-3}$), mF cm$^2$ | $n$ ($\pm10^{-2}$) |
|---|---|---|---|---|---|
| Blank | 1.6 | 43 | 695 | 203 | 0.72 |
| $1 \times 10^{-4}$ | 1.7 | 104 | 569 | 211 | 0.74 |
| $3 \times 10^{-4}$ | 1.6 | 143 | 353 | 140 | 0.75 |
| $5 \times 10^{-4}$ | 1.5 | 167 | 261 | 133 | 0.77 |
| $1 \times 10^{-3}$ | 1.6 | 197 | 251 | 125 | 0.76 |
| $2 \times 10^{-3}$ | 1.8 | 309 | 198 | 119 | 0.78 |

reported that the adsorption of organic inhibitor on the metal surface is characterized by a decrease in $C_{dl}$ [43]. The decreased values of $C_{dl}$ may be due to the replacement of water molecules at the electrode interface by organic inhibitor of lower dielectric constant through adsorption, suggesting that Schiff base inhibitor acts by adsorption at the metal-solution interface. The increase in values of $R_{ct}$ and the decrease in values of $C_{dl}$ with increasing concentration also indicate that Schiff base acts as a primary interface inhibitor and the charge transfer controls the corrosion of steel under the open circuit conditions [44].

### 3.2 Effect of Temperature

The effect of temperature on the inhibited acid–metal reaction is highly complex, because many changes occur on the metal surface such as rapid etching and desorption of inhibitor. This was accomplished by investigating the temperature dependence of the corrosion current, exploring the activation energy of the corrosion process and the thermodynamic functions of adsorption of PPPD. The activation parameters for the corrosion process were calculated from Arrhenius-type plot according to the following equation [44]:

$$\ln I_{corr} = \ln A - \frac{Ea}{RT}, \tag{21}$$

where $E_a$ is the apparent activation corrosion energy, $R$ is the universal gas constant, $A$ is the pre-exponential factor, and $T$ is the absolute temperature. Arrhenius plots for the corrosion density of carbon steel in the case of PPPD are given in Fig. 5. Values of apparent activation energy of corrosion ($E_a$) for steel in 1 M HCl with the absence and presence of various concentrations of PPPD were determined from the slope of $\ln(I_{corr})$ versus $T^{-1}$ plots and shown in Table 3. Inspection of the data shows that the activation energy is lower in the absence of inhibitors than in its presence. It has been reported that higher $E_a$ in the presence of inhibitor for steel in comparison with blank

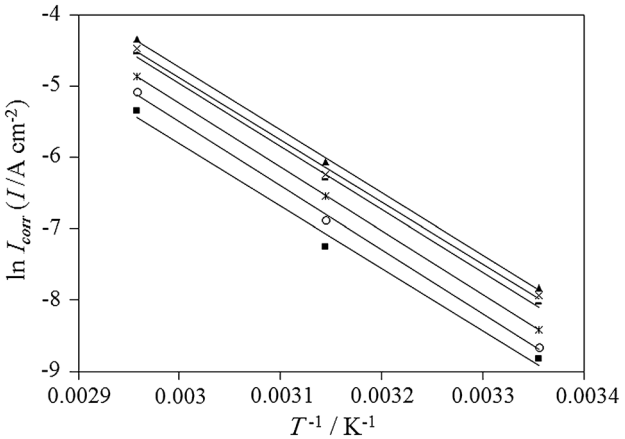


**Fig. 5** Typical Arrhenius plots of $\ln I_{corr}$ versus $T^{-1}$ for carbon steel in 1 M HCl at different concentrations of PPPD: 0 M (*filled triangle*), $1 \times 10^{-4}$ M (*times symbol*), $3 \times 10^{-4}$ M (*dash*), $5 \times 10^{-4}$ M (*asterisk*), $1 \times 10^{-3}$ M (*open circle*), $2 \times 10^{-3}$ M (*filled square*)

solution is typically showing physisorption [43]. An alternative formulation of Arrhenius equation is [44]:

$$I_{corr} = \left(\frac{RT}{Nh}\right) \exp\left(\frac{\Delta s_a}{R}\right) \exp\left(\frac{-\Delta H_a}{RT}\right), \tag{22}$$

where $h$ is Planck′s constant, $N$ is Avogadro's number, $\Delta S_a$ is the entropy of activation, and $\Delta H_a$ is the enthalpy of activation. Figure 6 shows a plot of $\ln(I_{corr}/T)$ against $1/T$. Straight lines are obtained with a slope of $(-\Delta H_a/R)$ and an intercept of $\ln(R/Nh) + \Delta S_a/R$ from which the values of $\Delta H_a$ and $\Delta S_a$ are calculated, which are listed in Table 3. In the system, the positive signs of the enthalpies $\Delta H_a$ reflect the endothermic nature of the steel dissolution process. Practically, $E_a$ and $\Delta H_a$ are of the same order. Large and negative values of entropies $\Delta S_a$ imply that the activated complex in the rate-determining step represents an association rather than a dissociation step, meaning that a decrease in disordering takes place on going from reactants to the activated complex [45, 46].

**Table 3** Activation parameters of the dissolution of steel in 1 M HCl solution in the absence and in the presence of PPPD

| Concentration, M | $E_a$ (±1), kJ mol$^{-1}$ | $A \times 10^9$ (±$10^3$), A cm$^{-2}$ | $\Delta S_a$ (±2), J mol$^{-1}$ | $\Delta H_a$ (±1), kJ mol$^{-1}$ | $E_a - \Delta H_a = RT$ (±1), kJ mol$^{-1}$ |
|---|---|---|---|---|---|
| Blank | 71.8 | 0.655 | −80 | 69.2 | 2.6 |
| $1 \times 10^{-4}$ | 86 | 2.81 | −43 | 83.4 | 2.6 |
| $3 \times 10^{-4}$ | 87 | 9.21 | −40 | 84.4 | 2.6 |
| $5 \times 10^{-4}$ | 89 | 81.7 | −36 | 86.4 | 2.6 |
| $1 \times 10^{-3}$ | 91.2 | 236 | −31 | 88.6 | 2.6 |
| $2 \times 10^{-3}$ | 92.1 | 500 | −30 | 89.5 | 2.6 |

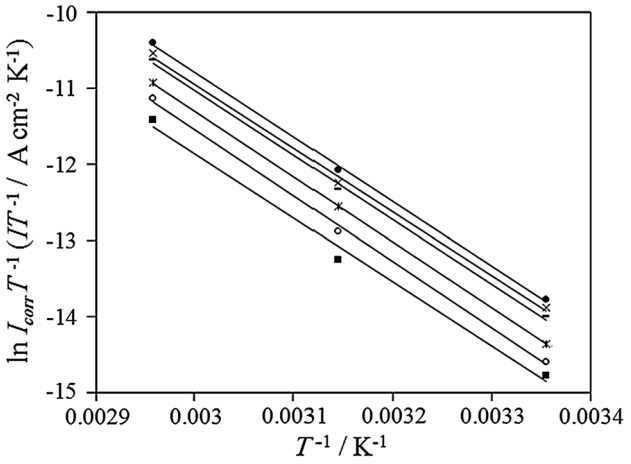


**Fig. 6** Typical Arrhenius plots of $\ln I_{corr}\ T^{-1}$ versus $T^{-1}$for carbon steel in 1 M HCl at different concentrations of PPPD: : 0 M (*filled circle*), $1 \times 10^{-4}$ M (*times symbol*), $3 \times 10^{-4}$ M (*dash*), $5 \times 10^{-4}$ M (*asterisk*), $1 \times 10^{-3}$ M (*open circle*), $2 \times 10^{-3}$ M (*filled square*)

### 3.3 Adsorption Isotherm and Thermodynamic Parameters

Adsorption isotherms provide information about the interaction of the adsorbed molecules with the metal surface [43]. The efficiency of Schiff base molecules as a successful corrosion inhibitor mainly depends on their adsorption ability on the metal surface. The adsorption process consists of the replacement of water molecules at a corroding interface according to following process [47].

$$\mathrm{Org}_{(sol)} + n\mathrm{H_2O}_{(ads)} \leftarrow \mathrm{Org}_{(ads)} + n\mathrm{H_2O}_{(sol)}, \quad (23)$$

where $\mathrm{Org}_{(sol)}$ and $\mathrm{Org}_{(ads)}$ are the organic molecules in the solution and adsorbed on the metal surface, respectively, and $n$ is the number of water molecules replaced by the organic molecules. It is essential to know the mode of adsorption and the adsorption isotherm that can give important information on the interaction of inhibitor and metal surface. Ten adsorption isotherms (Langmuir, Temkin, Freundlich, Frumkin, Modified, Langmuir, Henry, Viral, Damaskin, Volmer and Flory–Huggins) [48–50] were tested for their fit to the experimental data. The linear regression coefficient values ($R^2$) were determined from the plotted curves. According to these results, it can be concluded that the best description of the adsorption behavior of PPPD can be explained by Langmuir adsorption isotherm which is given by (Eq. 24):

$$\frac{C}{\theta} = \frac{1}{K_{ads}} + C, \quad (24)$$

where $\theta$ is the surface coverage degree, $C$ is the concentration of inhibitor, and $K_{ads}$ is the adsorptive equilibrium constant. The linear relationships of $C/\theta$ versus $C$, depicted in Fig. 7 suggest that the adsorption of PPPD on the steel surface obeyed the Langmuir adsorption isotherm in different temperatures. Langmuir's isotherm assumes that the adsorption of organic molecule on the adsorbent is monolayer and the adsorbed molecules occupy only one site and there are no interactions with other adsorbed species. The standard free energy of adsorption of inhibitor ($\Delta G_{ads}$) on steel surface can be evaluated with the following equation:

$$\Delta G_{ads} = -RT \ln(55.5K_{ads}). \quad (25)$$

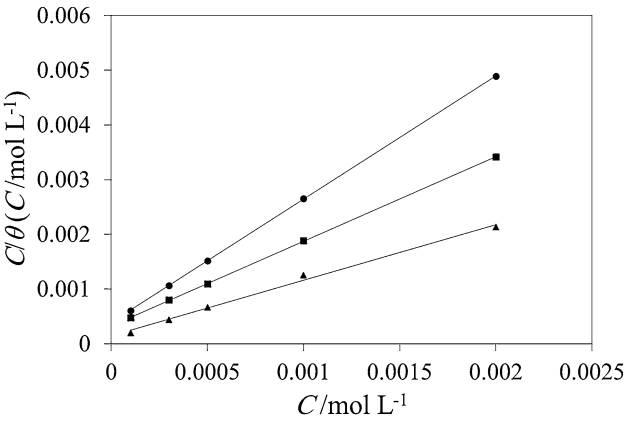


**Fig. 7** Langmuir adsorption plot for steel electrode in 1 M HCl at different temperatures: 25 °C (*filled triangle*), 45 °C (*filled square*), 65 °C (*filled circle*)

The value 55.5 in the above equation is the concentration of water in solution in mol $l^{-1}$ [51]. The negative values of $\Delta G_{ads}$ suggest that the adsorption of PPPD on the carbon steel surface is spontaneous. Generally, the values of $\Delta G_{ads}$ around or less than −30 kJ $mol^{-1}$ are associated with the electrostatic interaction between charged molecules and the charged metal surface (physisorption); while those around or higher than −40 kJ $mol^{-1}$ mean charge sharing or transfer from the inhibitor molecules to the metal surface to form a coordinate type of metal bond (chemisorption). The values of $K_{ads}$ and $\Delta G_{ads}$ are listed in Table 4. The $\Delta G_{ads}$ values are around −30 kJ $mol^{-1}$, which means that the absorption of PPPD on the carbon steel surface belongs to the physisorption and the adsorptive film has an electrostatic character [52]. Enthalpy and entropy of adsorption ($\Delta H_{ads}$ and $\Delta S_{ads}$) can be calculated using the following equation [40]:

$$\Delta G_{ads} = \Delta H_{ads} - T\Delta S_{ads} \quad (26)$$

$$\ln K_{ads} = -\frac{\Delta H_{ads}}{RT} + \frac{\Delta S_{ads}}{R} - \ln(55.5). \quad (27)$$

Figure 8 represents the plots of ln $K_{ads}$ versus $T^{-1}$ for adsorption PPPD. The lines obtained represent a slope of $(-\Delta H_{ads}/R)$ and intercept of $[(\Delta S_{ads}/R) - \ln(55.5)]$. Thermodynamic parameters for the adsorption of inhibitors can provide valuable information about the mechanism of corrosion inhibition. An endothermic adsorption process $\Delta H_{ads} > 0$ is attributed unequivocally to chemisorption, and the exothermic adsorption process $\Delta H_{ads} < 0$ may involve either physisorption or chemisorption or a mixture of both the processes. Based on the results of this study, the calculated $\Delta G_{ads}$ and $\Delta H_{ads}$ values for PPPD show that adsorption mechanism is not completely physical or chemical and a combination of physisorption and chemisorption exists between the inhibitor and metal surface. The positive sign of $\Delta S_{ads}$ arises from substitution process, which can be attributed to the increase in the solvent entropy and more positive water desorption entropy. It also interpreted with an increase of disorders due to more water molecules which can be desorbed from the metal surface by one inhibitor molecule [42].

**Table 4** Thermodynamic and equilibrium adsorption parameters for adsorption PPPD on carbon steel surface in 1 M HCl solution

| Temperature, K | $K_{ads}$ ($\pm 10^2$), l $mol^{-1}$ | $\Delta G_{ads}$ ($\pm 10^{-1}$), kJ $mol^{-1}$ |
|---|---|---|
| 298 | 4899 | −31.7 |
| 318 | 3431 | −32.2 |
| 338 | 2500 | −33.3 |

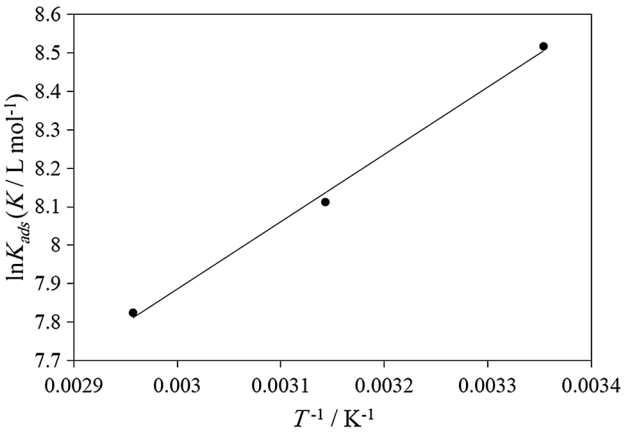


**Fig. 8** ln($K_{ads}$) versus $T^{-1}$ for adsorption PPPD on steel surface

### 3.4 Surface Metallography

AFM and scanning electron images of the steel after 6 h immersion in 1 M HCl solution with and without inhibitor are shown in Figs. 9 and 10. In the absence of inhibitor (Figs. 9a, 10a), the surface displayed a very irregular topography due to corrosion attack. The average roughness $R_a$ of steel in 1 M HCl solution without inhibitor was calculated as 1.41 μm by AFM (Fig. 9a). In the presence of PPPD, smoother surface was obtained and the $R_a$ value decreased to 183 nm (Fig. 9b) as a consequence of low corrosion damage and the protective formation of an inhibitor layer on steel surface. SEM images indicate that corrosion was inhibited in the presence of PPPD (Fig. 10b). This is in good agreement with the result obtained from the EIS tests that with the increasing of PPPD concentration in solution increase the exponent $n$ of the double-layer capacitance.

### 3.5 Molecular Structure and Quantum Chemical Calculation

#### *3.5.1 Non-protonated Inhibitors*

Optimized structure of investigated inhibitor are obtained at each level and represented in Fig. 11 at M062X/6-31G level in vacuum. For non-protonated inhibitors, quantum chemical descriptors are calculated by using Eqs. (1)-(9) and listed in Table 5.

In Table 5, numerical values of quantum chemical descriptors are given at M062X/6-31G level in vacuum for the mentioned inhibitor. Calculated results for each descriptor are too close to each other. There are not significant differences between each level. Some selected structural parameters are given in Table 6 at M062X/6-31G level.

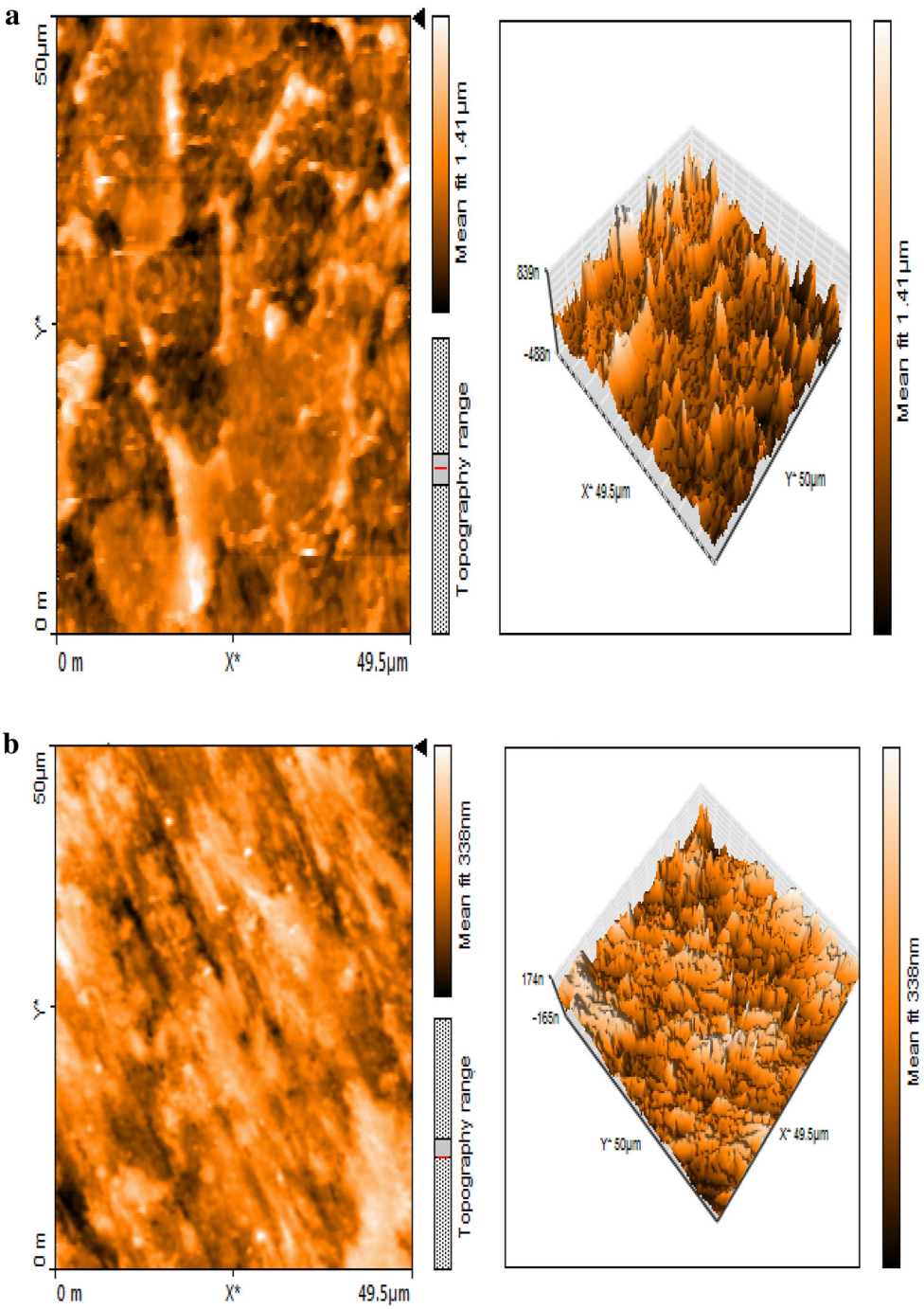


**Fig. 9** 2D and 3D of AFM images of carbon steel exposed to 1 M HCl solution **a** in the absence of $2 \times 10^{-3}$ M PPPD, **b** in the presence of $2 \times 10^{-3}$M PPPD. (scansize: 49.5 × 50 µm)

### *3.5.2 Investigation of Molecular Orbitals*

Inhibitor can coordinate to metal surface by donating or accepting electrons. Investigation of molecular orbitals, therefore, is important for determination of corrosion mechanism. If inhibitor donates electrons, these electrons donate from HOMO or HOMO−(n). If the energy level of HOMO and HOMO−(n) is close to each other, electrons are easily donated from HOMO−(n). On the other hand, electrons accept to LUMO or LUMO+(n), if inhibitor accepts electrons. Similar conditions can be said for LUMO and LUMO+(n). Energy diagram of around the frontier molecular orbitals (FMOs) are represented in Fig. 12. In this diagram, degeneracy tolerance is selected as 0.001 atomic unit (a.u).

According to Fig. 12, energy of LUMO and LUMO+1 are so close to each other and the energy of HOMO and HOMO−1 are so close to each other, too. These results

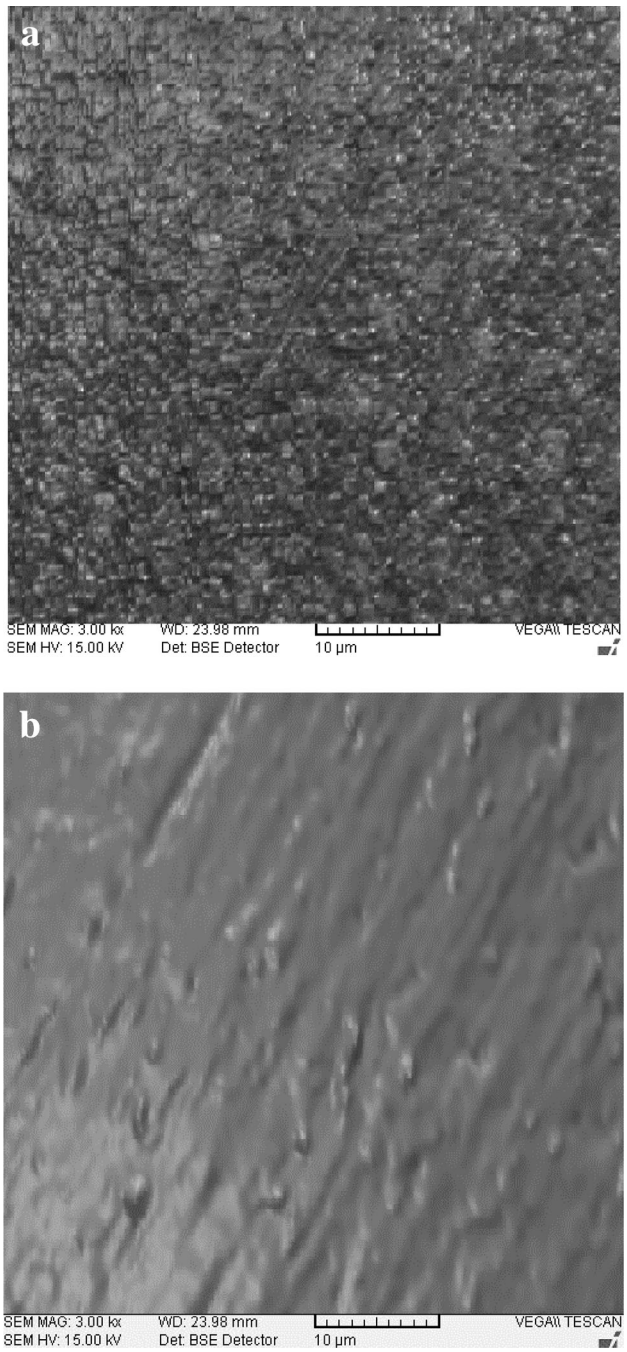


**Fig. 10** Surface of steel electrode by SEM microscope at in 1 M HCl solution **a** without and **b** with $2 \times 10^{-3}$ M PPPD

imply that electrons can be donated from HOMO or HOMO–1 while accepting to LUMO or LUMO+1.

### *3.5.3 Determination of Active Site*

Determination of active site in inhibitor is important to the mechanism of corrosion. Active sites of inhibitors can be determined with computational chemistry methods by using molecular electrostatic potential (MEP) maps, MEP contours, condensed Fukui functions, and local softness of heteroatoms in investigated inhibitor.

The greater value of Fukui functions mean that the highest active and Fukui functions provide important information which are the active sites for nucleophilic attacks, electrophilic attack, and radicalic attack in inhibitor and they are related to the highest $f_k^+$ value, highest $f_k^-$ value, and highest $f_k^0$ value, respectively. Additionally, tendencies of electron transferring of inhibitors toward metal surface can be discussed with hard and soft acid–base (HSAB) approximation and soft species are to be most effective for metallic bulks because the metallic bulk is softer than metal atoms. Beyond them, local softness values can be calculated for electrophilic attack ($\sigma^-$), radicalic attack ($\sigma^0$), and nucleophilic attack ($\sigma^+$). Condensed Fukui functions of heteroatoms and local softness are calculated M062X/6-31G levels in vacuo with Eqs. (10)–(15) and are listed in Table 7.

According to the Fukui functions, nitrogen atoms are appropriate for nucleophilic attack and oxygen atoms are appropriate for radicalic and electrophilic attack. On the other hand, nitrogen atoms are appropriate for nucleophilic and radical attack and oxygen atoms are appropriate for electrophilic attack.

Another method is the investigation of MEP maps and contour for determination of active sites. Different values of electrostatic potential at MEP map are represented by different colors. The red and yellow regions in MEP map are related to electrophilic active region and the light blue and blue regions in MEP map are related to nucleophilic active region. Additionally in MEP contours, there are two colors which are yellow and red and these color lines are related to positively charged and negatively charged regions, respectively. Steric effect can be easily seen from MEP contour. MEP maps and contours are represented in Fig. 13.

According to MEP maps of studied inhibitors, electrophilic active regions are mainly observed around the oxygen and nitrogen atoms which are located in the center of molecule. In MEP contours, electrons are mainly concentrated around the oxygen atoms which are labeled as 10O and 27O. As for the nitrogen atoms, hydrogen atoms which are coordinated to 10O and 27O atoms created steric effect around these atoms. This result implies that nitrogen atoms can be coordinated to metal surface only at appropriate position.

As a result, nitrogen atoms are appropriate for nucleophilic attacks and can be protonated for investigation of corrosion mechanism.

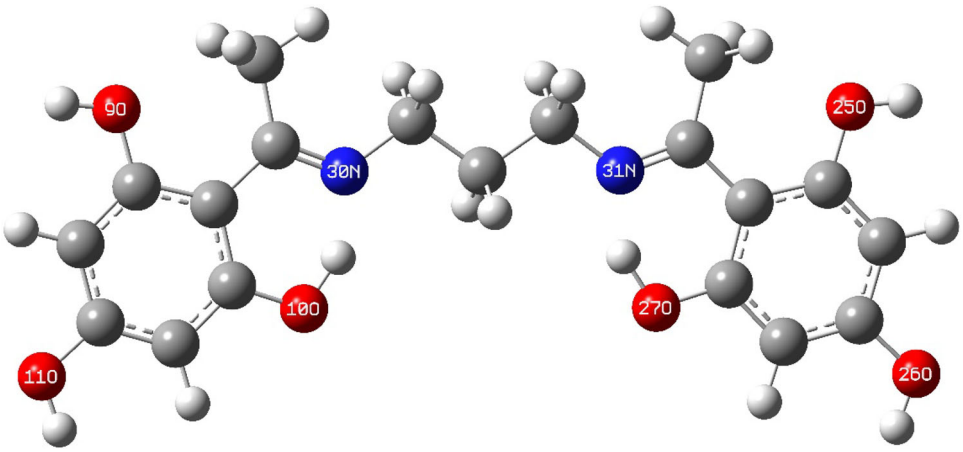


**Fig. 11** Optimized structures of investigated inhibitor at M062X/6-31G level in vacuum

**Table 5** Quantum chemical descriptors for non-protonated inhibitors and protonated forms at M062X/6-31G level

| | $E^{a}_{HOMO}$ | $E^{a}_{LUMO}$ | $E^{a}_{GAP}$ | $\eta^{a}$ | $\sigma^{b}$ | $\chi^{a}$ | $\omega^{a}$ | $N^{b}$ |
|---|---|---|---|---|---|---|---|---|
| Non-protonated | −7.051 | −0.062 | 6.989 | 3.494 | 0.286 | 3.556 | 1.810 | 0.553 |
| Protonated form (1) | −8.872 | −4.688 | 4.184 | 2.092 | 0.478 | 6.780 | 10.986 | 0.091 |
| Protonated form (2) | −8.872 | −4.688 | 4.184 | 2.092 | 0.478 | 6.780 | 10.986 | 0.091 |
| Protonated form (3) | −13.201 | −6.642 | 6.560 | 3.280 | 0.305 | 9.921 | 15.006 | 0.067 |

[a] In Ev

[b] In $eV^{-1}$

**Table 6** Optimized structural parameters of studied inhibitor at M062X/6-31G level in vacuum

| | | | |
|---|---|---|---|
| Bond lengths (Å) | | | |
| 9O–C | 1.386 | 27O–C | 1.344 |
| 10O–C | 1.344 | 30N=C | 1.303 |
| 11O–C | 1.379 | 31N=C | 1.303 |
| 25O–C | 1.386 | 10O–H–30N | 1.478 |
| 26O–C | 1.379 | 27O–H–31N | 1.478 |
| Bond Angle (°) | | | |
| 10O–H–30 N | 149.18 | 27O–H–31N | 149.18 |

### *3.5.4 Protonated Inhibitor*

Nitrogen atoms are determined as nucleophilic active site and can be used for protonation. Firstly, nitrogen atoms are protonated separately and then these atoms are protonated at the same time. Optimized structures of non-protonated and protonated inhibitors are represented in Fig. 14.

Optimized structures of protonated forms are represented in Fig. 14. Mentioned quantum chemical descriptors are given in Table 7. Proton affinity (PA) of non-protonated inhibitor is calculated by using Eqs. (16), (17) and are obtained as −270.31, −270.31, and −1084.26 kJ $mol^{-1}$ for protonated form (1), (2), and (3), respectively. Protonation effect on quantum chemical parameters can be easily seen from Table 7. According to these parameters and PA, nitrogen atoms are equal to each other in corrosion mechanism. Proton affinity in form (3) is more negative than the other forms. These results show that the inhibitor prefers to coordinate to metal surface by two nitrogen atoms at the same time.

## 4 Conclusion

The PPPD Schiff base was synthesized and investigated as corrosion inhibitor for carbon steel in 1 M HCl solution with different concentrations using a series of techniques. PPPD has a good inhibition effect for the corrosion of carbon steel in 1 M HCl solution especially in high concentration. Its inhibition efficiency is both concentration and temperature dependent. The high inhibition efficiency of Schiff base is attributed to the formation of a film on the steel surface. Corrosion current density is increased by increasing the temperature, but, the rate of its increase is lower at the presence of Schiff base compound. Polarization measurements demonstrate that PPPD behaved as mixed-type corrosion inhibitor by inhibiting both anodic metal dissolution and cathodic hydrogen evolution reactions. Impedance measurements indicate that with increasing inhibitor concentration, the polarization

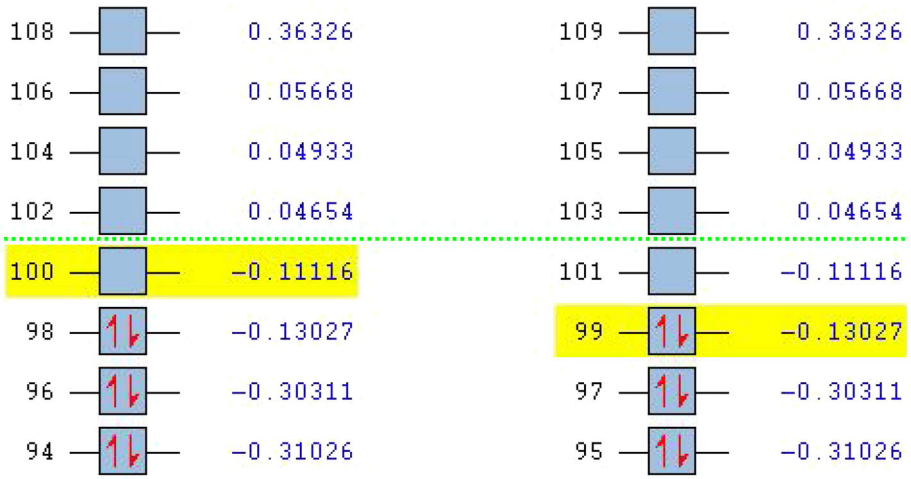


**Fig. 12** A section of electronic energy diagram of molecular orbital

**Table 7** Fukui functions and local softness of investigated inhibitor

| Heteroatoms | $P_k$ $(N-1)$ | $P_k$ $(N)$ | $P_k$ $(N+1)$ | $f_k^-$ | $f_k^0$ | $f_k^+$ | $\sigma^-$ | $\sigma^0$ | $\sigma^+$ |
|---|---|---|---|---|---|---|---|---|---|
| 9O | 8.709 | 8.715 | 8.734 | 0.006 | 0.012 | 0.019 | 0.002 | 0.004 | 0.005 |
| 10O | 8.642 | 8.724 | 8.757 | 0.082 | 0.057 | 0.033 | 0.023 | 0.016 | 0.009 |
| 11O | 8.687 | 8.722 | 8.732 | 0.035 | 0.022 | 0.010 | 0.010 | 0.006 | 0.003 |
| 25O | 8.709 | 8.715 | 8.734 | 0.006 | 0.012 | 0.019 | 0.002 | 0.004 | 0.005 |
| 26O | 8.687 | 8.722 | 8.732 | 0.035 | 0.022 | 0.010 | 0.010 | 0.006 | 0.003 |
| 27O | 8.642 | 8.723 | 8.757 | 0.082 | 0.057 | 0.033 | 0.023 | 0.016 | 0.009 |
| N30 | 7.523 | 7.473 | 7.611 | −0.050 | 0.044 | 0.138 | −0.014 | 0.013 | 0.039 |
| N31 | 7.523 | 7.469 | 7.611 | −0.054 | 0.044 | 0.141 | −0.015 | 0.013 | 0.040 |

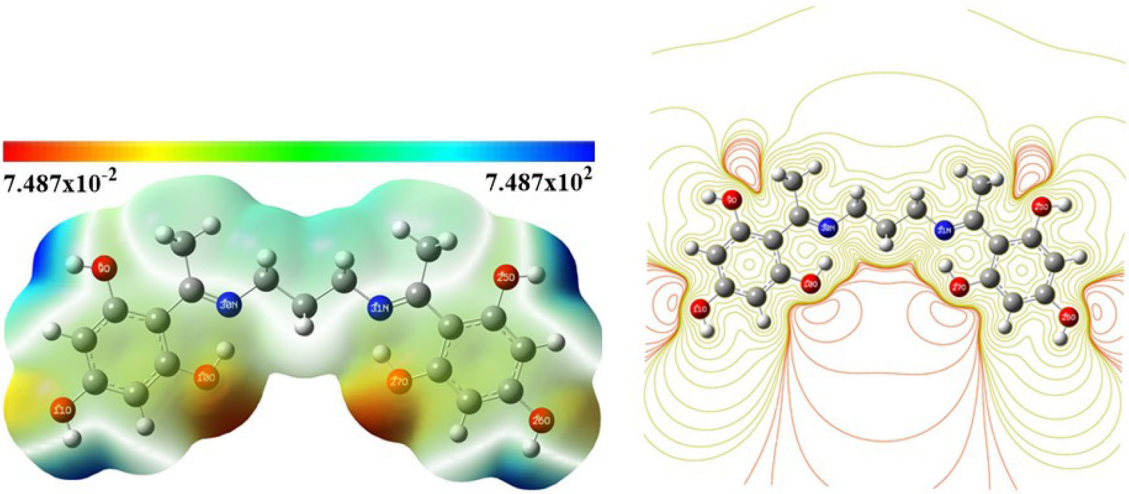


**Fig. 13** MEP maps and contours of investigated inhibitors at M062X method with 6-31G basis set in vacuum

resistance ($R_{ct}$) increased, while the double-layer capacitance ($C_{dl}$) decreased. The adsorption of PPPD molecules on carbon steel surface has been described by Langmuir adsorption isotherm. The values of $\Delta G_{ads}$ and $K_{ads}$ indicate the spontaneous interaction with surface and high adsorption ability of studied inhibitor. The high-resolution AFM and SEM micrographs showed that the corrosion of carbon steel in 1 M HCl solution was described by corrosion attack and the addition of inhibitor to the aggressive solutions diminished the corrosion of carbon steel. Quantum chemical calculations are performed on the studied inhibitor at M062X/6-31G level in vacuum. Energy

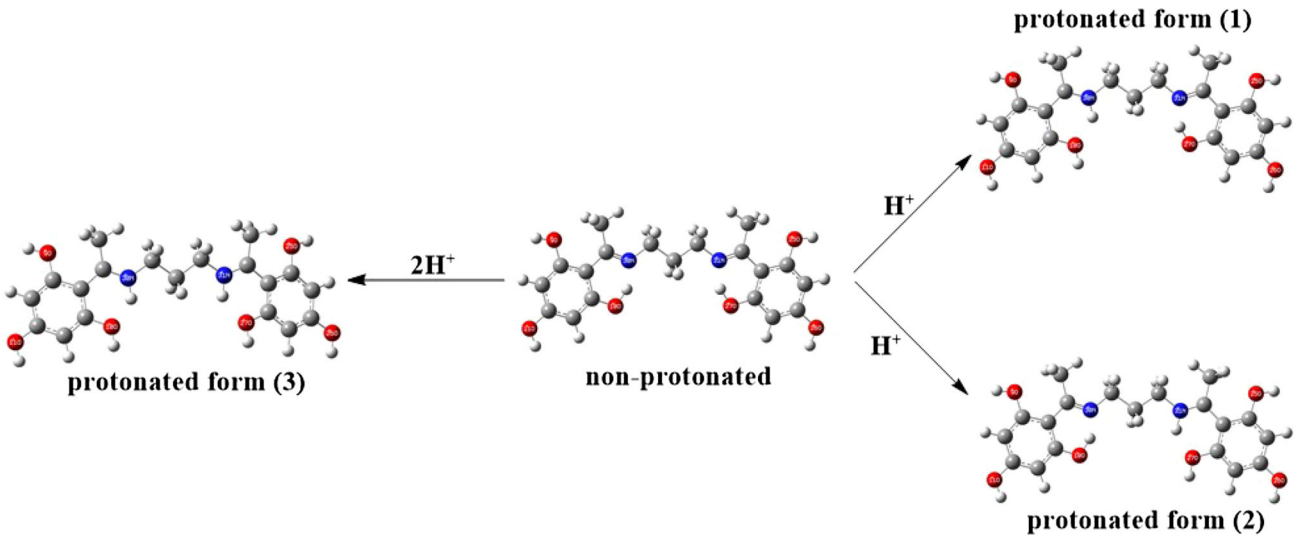


**Fig. 14** Protonated forms of investigated inhibitor at M062X/6-31G level in vacuum

diagrams of molecular orbitals are examined in detail and identical molecular orbitals are determined. Active sites or regions are investigated by condensed Fukui functions, local softness, and molecular electrostatic potential maps and contours. As it can be seen from Fukui functions which are represented in Table 7, nitrogen atoms are appropriate for nucleophilic attack. Firstly, nitrogen atoms are protonated separately and then protonated at the same time. Proton affinities are obtained as −270.31, −270.31, and −1084.26 kJ $mol^{-1}$ for the protonated forms (1), (2), and (3), respectively. These results show that the inhibitors prefer to coordinate to metal surface by two nitrogen atoms at the same time.

## References


1. Finšgar M, Jackson J (2014) Application of corrosion inhibitors for steels in acidic media for the oil and gas industry: a review. Corros Sci 86:17–41
2. Jafari H, Danaee I, Eskandari H, RashvandAvei M (2013) Electrochemical and theoretical studies of adsorption and corrosion inhibition of N, N′-bis(2-hydroxyethoxyacetophenone)-2,2-dimethyl-1,2-propanediimine on low carbon steel (API 5L grade B) in acidic solution. Ind Eng Chem Res 52:6617–6632
3. Osman MM, Shalaby MN (2003) Some ethoxylated fatty acids as corrosion inhibitors for low carbon steel in formation water. Mater Chem Phys 77:261–269
4. Okafor PC, Liu X, Zheng YG (2009) Corrosion inhibition of mild steel by ethylamino imidazoline derivative in $CO_2$-saturated solution. Corros. Sci. 51:761–768
5. Ebenso EE, Kabanda MM, Murulana LC, Singh AK, Shukla SK (2012) Electrochemical and quantum chemical investigation of some azine and thiazine dyes as potential corrosion inhibitors for mild steel in hydrochloric acid solution. Ind Eng Chem Res 51:12940–12958
6. Kabanda MM, Murulana LC, Ebenso EE (2012) Theoretical studies on phenazine and related compounds as corrosion inhibitors for mild steel in sulphuric acid medium. Int J Electrochem Sci 7:7179–7205
7. Negm NA, Elkholy YM, Zahran MK, Tawfik SM (2010) Corrosion inhibition efficiency and surface activity of benzothiazol-3-ium cationic Schiff base derivatives in hydrochloric acid. Corros Sci 52:3523–3536
8. Hasan BO, Sadek SA (2013) The effect of temperature and hydrodynamics on carbon steel corrosion and its inhibition in oxygenated acid–salt solution. J Ind Eng Chem 1300:11
9. Parr R, Yang W (1989) Density-functional theory of atoms and molecules. Oxford University Press, New York
10. Burke K, Perdew JP, Levy M (1995) Modern density functional theory: a tool for chemistry: theoretical and computational chemistry, vol 2. Elsevier Science, Amsterdam
11. Fairhurst SA, Hughes DL, Kleinkes U, Leigh GJ, Sanders JR, Weisner J (1995) J. Chem Soc Dalton Trans 321–326.
12. GaussView, Version 5, Roy Dennington, Todd Keith, and John Millam, Semichem Inc., Shawnee Mission, 2009.
13. Frisch MJ, Trucks GW, Schlegel HB, Scuseria GE, Robb MA, Cheeseman JR, Scalmani G, Barone V, Mennucci B, Petersson GA, Nakatsuji H, Caricato M, Li X, Hratchian HP, Izmaylov AF, Bloino J, Zheng G, Sonnenberg JL, Hada M, Ehara M, Toyota K, Fukuda R, Hasegawa J, Ishida M, Nakajima T, Honda Y, Kitao O, Nakai H, Vreven T, Montgomery JA, Jr, Peralta JE, Ogliaro F, Bearpark M, Heyd JJ, Brothers E, Kudin KN, Staroverov VN, Kobayashi R, Normand J, Raghavachari K, Rendell A, Burant JC, Iyengar SS, Tomasi J, Cossi M, Rega N, Millam JM, Klene M, Knox JE, Cross JB, Bakken V, Adamo C, Jaramillo J, Gomperts R, Stratmann RE, Yazyev O, Austin AJ, Cammi R, Pomelli C, Ochterski JW, Martin RL, Morokuma K, Zakrzewski VG, Voth GA, Salvador P, Dannenberg JJ, Dapprich S, Daniels AD, Farkas Ö, Foresman JB, Ortiz JV, Cioslowski J, Fox DJ (2013) Gaussian 09, Revision D.01. Gaussian, Inc., Wallingford
14. PerkinElmer (2012) ChemBioDraw ultra version (13.0.0.3015), CambridgeSoft, Waltham
15. Jafari H, Danaee I, Eskandari H, RashvandAvei M (2014) Combined computational and experimental study on the adsorption and inhibition effects of $N_2O_2$ schiff base on the corrosion of API 5L grade B steel in 1 mol/L HCl. J Mater Sci Technol 30:239–252

16. Jafari H, Danaee I, Eskandari H, RashvandAvei M (2013) Electrochemical and quantum chemical studies of N, N'-bis(4-hydroxybenzaldehyde)-2,2-dimethylpropandiimine Schiff base as corrosion inhibitor for low carbon steel in HCl solution. J Environ Sci Health A 48:1628–1641
17. Jafari H, Sayin K (2015) Electrochemical and theoretical studies of adsorption and corrosion inhibition of aniline violet compound on carbon steel in acidic solution. J Taiwan Inst Chem Eng 56:181–190
18. Obot IB, Gasem ZM (2014) Theoretical evaluation of corrosion inhibition performance of some pyrazine derivatives. Corr Sci 83:359–366
19. Sayin K, Karakaş D (2013) Quantum chemical studies on the some inorganic corrosion inhibitors. Corros Sci 77:37–45
20. Karakus N, Sayin K (2014) The investigation of corrosion inhibition efficiency on some benzaldehyde thiosemicarbazones and their thiole tautomers: Computational study. J Taiwan Inst Chem Eng 48:95–102
21. Jafari H, Sayin K (2015) Sulfur containing compounds as corrosion inhibitors for mild steel in hydrochloric acid solution. Trans Ind Inst Met. doi:10.1007/s12666-015-0556-2
22. Ashassi-Sorkhabi H, Shaabani B, Seifzadeh D (2005) Corrosion inhibition of mild steel by some schiff base compounds in hydrochloric acid. Appl Surf Sci 239:154–164
23. Chetouani A, Hammouti B, Benhadda T, Daoudi M (2005) Inhibitive action of bipyrazolic type organic compounds towards corrosion of pure iron in acidic media. Appl Surf Sci 249:375–385
24. Chetouani A, Aouniti A, Hammouti B, Benchat N, Benhadda T, Kertit S (2003) Corrosion inhibitors for iron in hydrochloride acid solution by newly synthesised pyridazine derivatives. Corros Sci 45:1675–1684
25. Emeregül KC, Hayval M (2006) Studies on the effect of a newly synthesized Schiff base compound from phenazone and vanillin on the corrosion of steel in 2 M HCl. Corros Sci 48:797–812
26. Satapathy AK, Gunasekaran G, Sahoo SC, Amit K, Rodrigues PV (2009) Corrosion inhibition by Justicia gendarussa plant extract in hydrochloric acid solution. Corros Sci 51:2848–2856
27. Olivares O, Likhanova NV, Gomez B, Navarrete J, Llanos-Serrano ME, Arce E, Hallen JM (2006) Electrochemical and XPS studies of decylamides of alphaamino acids adsorption on carbon steel in acidic environment. Appl Surf Sci 252:2894–2909
28. Abdel Rehim SS, Hazzazi OA, Amin MA, Khaled KF (2008) On the corrosion inhibition of low carbon steel in concentrated sulphuric acid solutions. Part I: chemical and electrochemical (AC and DC) studies. Corros Sci 50:2258–2271
29. Saleh MM, Atia AA (2006) Effects of structure of the ionic head of cationic surfactant on its inhibition of acid corrosion of mild steel. J Appl Electrochem 36:899–905
30. Gerengi H, Ibrahim Sahin H (2012) Schinopsis lorentzii extract as a green corrosion inhibitor for low carbon steel in 1 M HCl solution. Ind Eng Chem Res 51:780–787
31. Emregül KC, Atakol O (2003) Corrosion inhibition of mild steel with schiff base compounds in 1 M HCl. Mater Chem Phys 82:188–193
32. Li XH, Deng SD, Fu H (2010) Inhibition by *Jasminum nudiflorum* Lindl. leaves extract of the corrosion of cold rolled steel in hydrochloric acid solution. J Appl Electrochem 40:1641–1649
33. Larabi L, Harek Y, Traianel M, Mansri A (2004) Synergistic influence of poly(4-vinylpyridine) and potassium iodide on inhibition of corrosion of mild steel in 1 M HCl. J Appl Electrochem 34:833–839
34. Mansfeld F, Kendig MW, Tsai S (1982) Recording and analysis of AC impedance data for corrosion studies 2 experimental approach and results. Corrosion 38:570–580
35. Shih H, Mansfeld F (1989) A fitting procedure for impedance data of systems with very low corrosion rates. Corros Sci 29:1235–1240
36. Martinez S, Metikoš-Huković M (2003) A nonlinear kinetic model introduced for the corrosion inhibitive properties of some organic inhibitors. J Appl Electrochem 33:1137–1142
37. Danaee I, Noori S (2011) Kinetics of the hydrogen evolution reaction on NiMn graphite modified electrode. Int J Hydrog Energy 36:12102–12111
38. Aramaki K, Hagiwara M, Nishihara H (1987) A study on the oxidative-addition reaction of benzyl compounds in sulphuric acid and its relation to corrosion inhibition. Corros Sci 5:487–499
39. Aljourani J, Raeissi K, Golozar MA (2009) Benzimidazole and its derivatives as corrosion inhibitors for mild steel in 1 M HCl solution. Corros Sci 51:1836–1843
40. Obot IB, Obi-Egbedi NO (2011) Anti-corrosive properties of xanthone on mild steel corrosion in sulphuric acid: experimental and theoretical investigations. Curr Appl Phys 11:382–392
41. Herrag L, Chetouani A, Elkadiri S, Hammouti B, Aouniti A (2008) Pyrazole derivatives as corrosion inhibitors for steel in hydrochloric acid, Portugal. Ectrochim Acta 26:211–220
42. Jafari H, Akbarzade K, Danaee I (2014) Corrosion inhibition of carbon steel immersed in a 1 M HCl solution using benzothiazole derivatives. Arab J Chem, Arab. doi:10.1016/j.arabjc.2014.11.018
43. Martinez S, Stern I (2002) Thermodynamic characterization of metal dissolution and inhibitor adsorption processes in the low carbon steel/mimosa tannin/sulfuric acid system. Appl Surf Sci 199:83–89
44. Bockris JOM, Reddy AKN (1976) Modern electrochemistry, vol 2. Plenum Publishing Corporation, New York
45. Oguzie EE, Unaegbu C, Ogukwe CN, Okolue BN, Onuchukwu AI (2004) Inhibition of mild steel corrosion in sulphuric acid using indigo dye and synergistic halide additives. Mater Chem Phys 84:363–368
46. Bellman C (2008) Stamm M Polymer surfaces and interfaces. Springer, Berlin
47. Mu G, Li X, Qu Q, Zhou J (2006) Molybdate and tungstate as corrosion inhibitors for cold rolling steel in hydrochloric acid solution. Corros Sci 48:445–459
48. Flis J, Zakroczymski T (1996) Impedance characterization of the activation of iron surface for hydrogen entry from alkaline solution. J Electrochem Soc 41:1245–1250
49. Donahue FM, Nobe K (1965) Theory of organic theory of corrosion inhibitors: adsorption and linear free energy relationships. J Electrochem Soc 112:886–891
50. Kamis E, Bellucci F, Latanision RM, El-Ashry ESH (1991) Acid corrosion inhibition of nickel by 2-(triphenosphoranylidene) succinic anhydride. Corrosion 47:677–687
51. Li XH, Deng SD, Fu H, Mu GN (2009) Synergistic inhibition effect of rare earth cerium(IV) ion and sodium oleate on the corrosion of cold steel in $H_2SO_4$ solution. Corros Sci 51:2639–2651
52. Bentiss F, Lebrini M, Vezin H, Chai F, Traisnel M, Lagrené M (2009) Enhanced corrosion resistance of carbon steel in normal sulfuric acid medium by some macrocyclic polyether compounds containing a 1,3,4-thiadiazole moiety: AC impedance and computational studies. Corros Sci 51:2165–2173